

Microcirculation and Microvasculature in Breast Tumors: Pharmacokinetic Analysis of Dynamic MR Image Series

Gunnar Brix,^{1*} Fabian Kiessling,² Robert Lucht,¹ Susanne Darai,³ Klaus Wasser,² Stefan Delorme,² and Jürgen Griebel¹

The purpose of this study was to quantify microcirculation and microvasculature in breast lesions by pharmacokinetic analysis of Gd-DTPA-enhanced MRI series. Strongly T_1 -weighted MR images were acquired in 18 patients with breast lesions using a saturation-recovery-TurboFLASH sequence. Concentration-time courses were determined for blood, pectoral muscle, and breast masses and subsequently analyzed by a two-compartment model to estimate plasma flow and the capillary transfer coefficient per unit of plasma volume (F/V_p , K_{ps}/V_p) as well as fractional volumes of the plasma and interstitial space (f_p , f_i). Tissue parameters determined for pectoral muscle ($f_p = 0.04 \pm 0.01$, $f_i = 0.09 \pm 0.01$, $F/V_p = 2.4 \pm 1.3 \text{ min}^{-1}$, and $K_{ps}/V_p = 1.2 \pm 0.5 \text{ min}^{-1}$) and 10 histologically proven carcinomas ($f_p = 0.20 \pm 0.07$, $f_i = 0.34 \pm 0.16$, $F/V_p = 2.4 \pm 0.7 \text{ min}^{-1}$, and $K_{ps}/V_p = 0.86 \pm 0.62 \text{ min}^{-1}$) agreed reasonable well with literature data. Best separation between malignant and benign lesions was obtained by the ratio K_{ps}/F (0.35 ± 0.17 vs. 1.23 ± 0.65). The functional imaging technique presented appears promising to quantitatively characterize tumor pathophysiology. Its impact on diagnosis and therapy management of breast tumors, however, has to be evaluated in larger patient studies. Magn Reson Med 52:420–429, 2004. © 2004 Wiley-Liss, Inc.

Key words: dynamic MRI; breast tumors; contrast media; blood flow; capillary permeability

Breast cancer represents the most common malignancy in females, constituting a major health problem, particularly in developed countries. Conventional X-ray mammography, supplemented by sonography, has been proven to be the primary modality for breast imaging. However, despite the important role played by X-ray mammography as a diagnostic and screening tool, it suffers especially from a limited specificity and thus leads to unnecessary breast biopsies. Therefore, new noninvasive imaging strategies are required for discriminating between benign and malignant breast masses in women with equivocal findings in conventional breast imaging or women with breast implants, previous therapy, or predisposing mutations of tumor suppressor genes. Besides positron emission tomog-

raphy (PET), dynamic contrast-enhanced MRI is the most promising approach providing information on tumor pathophysiology for improved diagnosis and management of breast lesions.

As summarized in recent review articles on dynamic MR mammography (1–3), the kinetics of signal variation in breast lesions after injection of a paramagnetic contrast medium (CM) represents an important criterion for the detection and differentiation of suspicious breast masses. According to the analysis presented by Kuhl et al. (4), a persisting (accumulating) enhancement pattern or a wash-out phenomenon over a period of time of about 5–6 min after the initial perfusion phase is a strong indicator for benign and malignant lesions, respectively.

Although the histopathological basis of the different enhancement patterns in breast masses is not yet fully understood, it is well known that angiogenesis, i.e., the formation of new vessels, is an important aspect (5,6). Microvessels in solid tumors exhibit a series of severe structural and functional abnormalities: They are often dilated, tortuous, elongated, and saccular and show an incomplete or even missing endothelial lining and an interrupted basement membrane. Moreover, there is an anarchic vascular organization of microvessels accompanied by significant arterio-venous shunt flow (6).

To gain further insight into contrast enhancement in breast lesions and its histopathological basis, it is necessary to study tumor microvasculature and microcirculation in more detail in vivo. To this end, various MR studies were performed to quantify different aspects of contrast enhancement using either simple compartment models or principles of indicator-dilution theory (7–15). With the exception of a double-tracer method used in an animal model (14), these techniques, however, do not allow distinguishing between the two relevant physiological transport processes, namely, the transport of CM through tissue vasculature by regional blood flow and its permeation across microvascular walls into the interstitial space. Therefore, it was the aim of this study to investigate the applicability and potential of a compartment approach (16), which offers the possibility to estimate regional blood flow and capillary permeability as well as volume fractions of the intravascular and interstitial space.

PATIENTS AND METHODS

Patients

The population examined in this study included 18 females ages 27–81 years (mean age, 50.4 years) with suspicious breast lesions detected by means of physical examination (inspection, palpation), X-ray mammography, and/or sonography. Exclusion criteria were pregnancy at

¹Division of Medical Radiation Hygiene and Dosimetry, Department of Radiation Protection and Health, Federal Office for Radiation Protection, Oberschleissheim, Germany.

²Research Program 'Innovative Diagnosis and Therapy,' German Cancer Research, Center (DKFZ), Heidelberg, Germany.

³Department of Gynaecological Radiology, University of Heidelberg, Germany.

Grant sponsor: German Cancer Aid (Deutsche Krebshilfe); Grant number: 70–2323.

*Correspondence to: Priv.-Doz. Dr. Gunnar Brix, Abteilung für Medizinische Strahlenhygiene und Dosimetrie, Bundesamt für Strahlenschutz, Ingolstädter Landstraße 1, D-85764 Oberschleissheim, Germany. E-mail: gbrix@bfs.de
Received 17 December 2003; revised 2 March 2004; accepted 26 March 2004.

DOI 10.1002/mrm.20161

Published online in Wiley InterScience (www.interscience.wiley.com).

© 2004 Wiley-Liss, Inc.

the time of study and the presence of metal implants. Breast lesions were either proved by histology following breast biopsy/surgery or, in the case of two fibroadenomas, by follow-up examinations over more than 9 months. The study was approved by the institution's Human Ethics Committee. Moreover, written informed consent was obtained from all patients after the nature of the procedure had been fully explained.

MR Imaging

MR imaging was performed with a 1.5 T whole-body MR system (MAGNETOM Vision; Siemens, Erlangen, Germany) using the circular-polarized body coil for RF transmission and a double-breast coil for RF detection. The patients lay prone on the breast coil with the arms extended above the head.

In the first step, precontrast 3D FLASH images were acquired (repetition time, $TR = 12$ ms; echo time, $TE = 5$ ms; flip angle, $\alpha = 35^\circ$; slice thickness, $TH = 4$ mm; matrix size = 256×256 ; field of view (FOV) = 320 mm; 32 transaxial slices). On the basis of these static images, two transaxial sections were defined ($FOV = 320$ mm, $TH = 6$ mm) crossing the lesion and the aorta for further evaluation.

In order to estimate precontrast T_1 relaxation times of blood, pectoral muscle, and breast lesions, seven T_1 -weighted images were acquired from each slice before CM administration in eight consecutive patients using a specially optimized saturation-recovery-TurboFLASH (SRTF) sequence ($TR = 10$ ms, $TE = 4.1$ ms, $\alpha = 12^\circ$, raw matrix size = 256×128 , image matrix size = 256×256) with recovery times of $T_{REC} = 100, 300, 600, 900, 1200, 1500, 3000$ ms. Preparation of the spin system was done by six nonselective 90° pulses, separated by intervals of decreasing length, during which the actual transversal magnetization was dephased by gradient spoiler pulses. This preparation scheme resulted in an almost complete cancellation of the longitudinal magnetization, even in the case of an imperfect magnetic RF field (7).

Using the same sequence, strongly T_1 -weighted ($T_{REC} = 125$ ms) images were acquired from the same cross s before, during, and after intravenous administration of 0.1 mmol Gd-DTPA (MAGNEVIST; Schering AG, Berlin, Germany) per kg body weight at a constant rate over 30 s with an infusion pump (CAI 626P/Tomojet; Doltron AG, Uster, Switzerland). In all patients, 128 images were measured per slice over a period of 6.9 min with an interval of 3.25 s between successive images. After a pause of ~ 80 s, required for image reconstruction and storage, 40 SRTF images per slice were additionally acquired in eight consecutive patients with the same sequence and timing.

Image Postprocessing

Image postprocessing was performed on a personal computer using IDL (Interactive Data Language, v. 5.2, Research Systems, Boulder, CO). As a first step towards a more sophisticated kinetic analysis, the spatial pattern of contrast enhancement was displayed. To this end, a color-coded parameter map per slice was computed from the initially acquired 128 SRTF images by means of a simple

kinetic model used in previous studies (7). Based on the color-coded maps, which visualize both the degree and rate of MR signal enhancement, regions of interest (ROIs) were placed over the central part of the aorta, the pectoral muscle, and the region within the breast lesion with the highest and fastest enhancement. The ROIs were transferred to the corresponding T_1 -weighted SRTF images to compute average signal intensities as a function of the recovery or measurement time, respectively.

Conversion of Signal–Time Courses Into Concentration–Time Courses

Signal analysis was performed with the program package SigmaPlot (v. 7.101; SPSS, Chicago, IL).

As shown theoretically and by phantom experiments (7,17), the signal intensity S of images acquired with the SRTF sequence can be described in a good approximation by:

$$S = \rho[1 - \exp(-T_{REC}/T_1)], \quad [1]$$

where ρ is the T_2^* -weighted proton density and T_1 the longitudinal relaxation time. After administration of a paramagnetic CM, T_1 has to be replaced under “fast exchange” conditions (18) by:

$$\frac{1}{T_{1CM}(t)} = \frac{1}{T_{10}} + \alpha C_T(t), \quad [2]$$

with T_{10} the tissue specific precontrast relaxation time, α the frequency-dependent relaxivity of the CM in plasma ($4.3 \text{ mM}^{-1} \text{ s}^{-1}$ for Gd-DTPA at 1.5 T and 37°C (19)), and C_T the average CM concentration in the tissue. According to Eqs. [1] and [2], concentration-time courses can be computed from the measured signal-time courses by:

$$C_T(t) = \frac{-1}{T_{REC}\alpha} \cdot \ln \left[\frac{S_{CM}(t)}{S_0} - \exp(T_{REC}/T_{10}) \cdot \left(\frac{S_{CM}(t)}{S_0} - 1 \right) \right] \quad [3]$$

with S_0 the precontrast signal.

Precontrast relaxation times T_{10} of blood, pectoral muscle, and breast lesions were estimated in eight patients from the SRTF data acquired with different recovery times by a nonlinear regression analysis according to Eq. [1]. For blood and muscle tissue, the average T_{10} value was calculated and used to estimate the corresponding tissue concentrations for all females by means of Eq. [3]. In contrast to normal tissues, breast lesions are characterized by a much greater inter- and intraindividual variability, and thus individual T_{10} values must be measured as pointed out by Tofts et al. (8). In order to avoid additional measurements and thus an elongation of the overall measurement time in routine breast imaging, we investigated an alternative approach to determine precontrast T_1 times of breast lesions directly from the precontrast values S_0 of the acquired signal–time courses. The approximation method is based on the observation that a Taylor expansion of Eq. [1] gives a linear relationship between the precontrast signal S_0 and the longitudinal relaxation rate $1/T_{10}$ for $T_{REC} \ll T_1$ as realized in the present study. The same holds

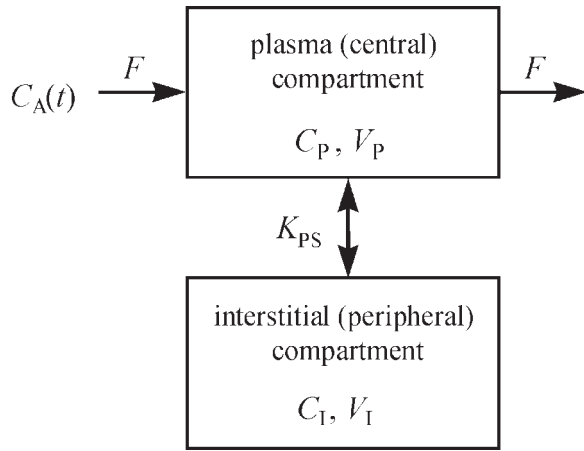


FIG. 1. Two-compartment model to describe the transport of Gd-DTPA through capillaries and its bidirectional transport between plasma (mean concentration, C_P ; volume, V_P) and interstitial space (mean concentration, C_I ; volume, V_I). $C_A(t)$ is the plasma concentration in a tissue feeding artery, F the capillary plasma flow, and K_{PS} the capillary transfer coefficient.

true for the relative signal S_0/S_0^{fat} , where S_0^{fat} is the SRTF signal evaluated in a fatty tissue region near the breast lesion considered, since interindividual variations in fatty tissue are negligible in good approximation. In contrast to the absolute signal S_0 of a lesion, the relative signal S_0/S_0^{fat} does not depend on the actual adjustment of the MR system, and image scaling and thus a linear relation:

$$1/T_{10} = k \cdot S_0^{\text{lesion}}/S_0^{\text{fat}}, \quad [4]$$

can be established, which makes it possible to estimate the precontrast relaxation rate of a breast lesion directly from the signal ratio S_0/S_0^{fat} . The proportionality factor k was determined by linear correlation analysis using the T_{10} values evaluated in eight women as described above. Correlation between both variables was tested at a significance level of $P = 0.05$ by calculating Spearman's rank correlation coefficient r_s (SigmaStat; v. 2.03; SPSS).

Pharmacokinetic Modeling

The pharmacokinetic model used to analyze the concentration–time courses measured in tissue is shown in Fig. 1; a detailed derivation of the model was presented in a previous article (16). According to this open two-compartment model, tracer transport through the capillary plasma compartment (with mean CM concentration C_P and volume V_P) and its transport into the interstitial space (with mean concentration C_I and volume V_I) is described by the following pair of mass balance equations:

$$V_P \frac{dC_P(t)}{dt} = F(C_A - C_P) - K_{PS}(C_P - C_I), \quad [5]$$

and

$$V_I \frac{dC_I(t)}{dt} = K_{PS}(C_P - C_I), \quad [6]$$

where F is the capillary plasma flow and K_{PS} the capillary transfer coefficient. Mean concentrations of the extracellular CM in arterial blood plasma $C_A(t)$ (the arterial input function), $C_B(t)$, determined from the dynamically acquired MRI datasets by $C_A(t) = C_B(t)/(1 - h_{mv})$ with $h_{mv} \approx 0.45$ the hematocrit in major vessels. The total tissue concentration, C_T , related to the measurable increase of the MR signal according to Eq. [3], is given by:

$$C_T(t) = f_P C_P(t) + f_I C_I(t), \quad [7]$$

where $f_P = V_P/V_T$ and $f_I = V_I/V_T$ are the volume fractions of the plasma and the interstitial distribution space within the examined tissue volume V_T , respectively.

Pharmacokinetic analysis was performed with the program MKMODEL (v. 5.0, Biosoft, Cambridge, UK) using the model described by Eqs. [5–7]. The following independent tissue parameters were estimated (besides the lag-time) from the concentration–time courses $C_T(t)$ and $C_A(t)$: F/V_P , K_{PS}/V_P , f_P , and f_I (note: $K_{PS}/V_I = K_{PS}/V_P \cdot f_P/f_I$). Errors in the final fit parameters were computed via the covariance matrix.

According to the complex mathematical analysis presented in Refs. 20,21, the mean residence times for CM particles passing through the plasma compartment and the interstitial compartment are given by:

$$MRT_P = \frac{V_P}{F} \quad \text{and} \quad MRT_I = \frac{V_I}{F} = \frac{f_I}{f_P} \cdot \frac{V_P}{F}. \quad [8]$$

The sum is the system mean residence time MRT_S

$$MRT_S = \frac{V_P + V_I}{F} = MTT_S, \quad [9]$$

which equals the system mean transit time MTT_S . Whereas the mean transit time gives the average time required by a CM particle to flow from the inlet of a (sub)system to its outlet (by whatever path), the residence time refers to the time that a particle remains in the compartment under study. Transit and residence times are identical for (sub-)systems if all material leaving cannot reenter. Since both quantities refer to an infinitely short CM input, there is per definition no reentry of CM when considering the system as a whole, and thus $MRT_S = MTT_S$.

To be comparable with data presented by other groups, the regional blood volume per unit tissue mass rBV (in ml/100 g) and the regional blood flow per unit tissue mass rBF (in ml/min/100 g) was computed according to:

$$rBV = \frac{V_P}{(1 - h_{sv}) \cdot m} = \frac{f_P}{(1 - h_{sv}) \cdot \rho} \quad [10]$$

and

$$rBF = \frac{F}{(1 - h_{sv}) \cdot m} = rBV \cdot \frac{F}{V_P} \quad [11]$$

where $h_{sv} \approx 0.25$ is the hematocrit in small vessels and $m = \rho V_T$ is the mass of the soft tissue with density $\rho = 1.04 \text{ g/cm}^3$ in the examined tissue volume V_T .

To investigate the potential of the pharmacokinetic analysis presented, model parameters were estimated for all women from concentration–time courses with 128 data points acquired every 3.25 s over 6.9 min. The significance of differences in the estimated tissue parameters of benign and malignant lesions was tested by applying the Mann-Whitney rank sum test at a significance level of $P = 0.05$. To assess the effect of different measurement strategies on the accuracy of parameter estimation, different reduced datasets were derived from the concentration–time curves measured in eight breast lesions with a sampling time of 3.25 s over the long acquisition time of 10.4 min (reference strategy, S1) by omitting data points. By this approach, the following five sampling strategies S2–S6 (characterized by the tuple “total acquisition time/sampling time”) were simulated: S2: 10.4 min / 6.5 s, S3: 10.4 min / 13.0 s, S4: 10.4 min / 26.0 s, S5: 6.9 min / 3.25 s, and S6: 3.45 min / 3.25 s. For each sampling strategy, the evaluation yielded different estimates $X_{ij}^{(S)}$ for the $i = 1, \dots, 4$ fit parameters (f_p , f_l , F/V_p , and K_{ps}/V_p) and the $j = 1, \dots, 8$ lesion considered. To evaluate the sampling strategies S2–S6 against the reference strategy S1, the mean relative deviation:

$$\delta^{(S)} = \frac{1}{32} \sum_{i=1}^4 \sum_{j=1}^8 \left| \frac{X_{ij}^{(S)} - X_{ij}^{(1)}}{X_{ij}^{(1)}} \right| \quad [12]$$

was computed.

RESULTS

Histological evaluation of suspicious breast masses in 16 patients yielded nine ductal invasive carcinomas, one lobular invasive carcinoma, five fibroadenomas, and one inflammatory lesion. The other two women suffered from a known fibroadenoma with a diameter of 26 mm and 31 mm, respectively. The widest diameter of all examined lesions was 24 ± 11 mm (mean \pm SD; range, 8–53 mm).

For blood and pectoral muscle, nonlinear regression analysis yielded precontrast T_1 values of 1348 ± 94 ms (range, 1222–1487 ms) and 607 ± 85 (range, 458–699 ms), respectively. In Fig. 2, the T_1 relaxation rates evaluated by nonlinear regression analysis in eight breast lesions are plotted vs. the corresponding lesion-to-fat signal ratios. Linear regression analysis yielded a slope of $k = 2.83 \text{ s}^{-1}$ for the regression line. Statistical analysis confirmed a highly significant linear correlation between both quantities ($P < 0.001$, $r_S = 0.952$), which justifies the approximation method for T_1 determination described by Eq. [4]. Based on the established regression line, T_1 values of between 558–1030 ms were estimated for the 18 breast lesions. Relaxation times were slightly lower for the 10 carcinomas (770 ± 146 ms) than for the 8 benign lesions (875 ± 107 ms).

The independent model parameters f_p , f_l , F/V_p , and K_{ps}/V_p determined for the six different sampling strategies S1–S6 are plotted in Fig. 3 for eight breast lesions. The mean relative deviations $\delta^{(S)}$ between the fit parameters

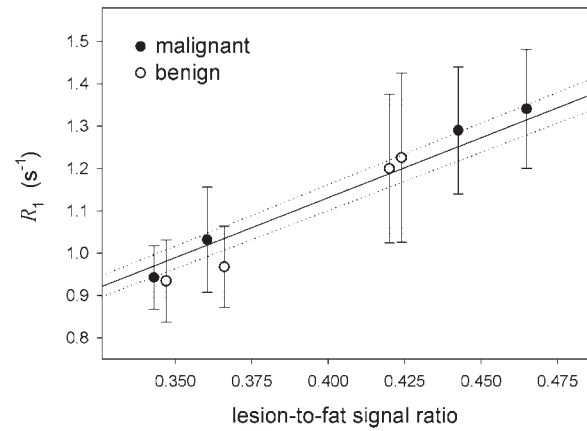


FIG. 2. Relation between precontrast relaxation rates $R_1 = 1/T_1$ and lesion-to-fat signal ratios measured in four breast carcinomas and four fibroadenomas. Symbols and error bars represent T_1 values and corresponding uncertainties, respectively, estimated by a nonlinear least-squares fit. The solid line gives the result of a linear regression analysis through the origin and the dotted curves the 95% confidence interval.

determined for the sampling strategies S2–S6 and those for the reference strategy S1 were 8.4% (S2 vs. S1), 25.1% (S3 vs. S2), 22.8% (S4 vs. S1), 10.8% (S5 vs. S1), and 62.6% (S6 vs. S1).

In Fig. 4 the fit parameters f_p , f_l , F/V_p , and K_{ps}/V_p estimated from concentration–time curves acquired over 6.9 min with a sampling time of 3.25 s (strategy S5) as well as the corresponding derived parameters rBV , rBF , MRT_p , MRT_l , f_l/f_p , and K_{ps}/F are presented separately for the 10 malignant and the 8 benign lesions. Significant differences in the median values between the two groups were found for f_p , F/V_p , rBV , rBF , MRT_p , MRT_l , and K_{ps}/F . Best separation between malignant and benign lesions was obtained by the ratio K_{ps}/F (0.35 ± 0.17 vs. 1.23 ± 0.65). Choosing a cut-off level of $K_{ps}/F = 1$, the 10 carcinomas and 6 of 8 benign lesions were classified correctly.

To illustrate the quantitative results, representative concentration–time curves determined from the aorta, two fibroadenomas, and two carcinomas are presented in Fig. 5 along with the fitted model parameters. The average peak concentration in blood plasma was 1.2 ± 0.2 mM (range, 0.72–1.49 mM). Concentration–time courses of breast masses show a variable pattern: After a fast initial increase, the curves show either a further slow increase (Fig. 5b,e) or a slow decrease (Fig. 5c,d) over a period of about 5 min. As demonstrated by the plots, this behavior can be explained physiologically by separating the bulk tissue concentration into its plasma and interstitial component. Lesions with a continuously increasing bulk tissue CM concentration after the initial perfusion phase had a volume ratio f_l/f_p of 4.2 ± 2.6 (range, 1.3–9.1) and those with an almost constant or decreasing concentration of 1.0 ± 0.2 (0.8–1.3).

Signal enhancement observed in the pectoral muscle upon Gd-DTPA administration was markedly lower than that found in breast masses. Due to the resulting poor signal-to-noise ratio of the dynamically acquired MR data, the concentration–time courses could not be analyzed on

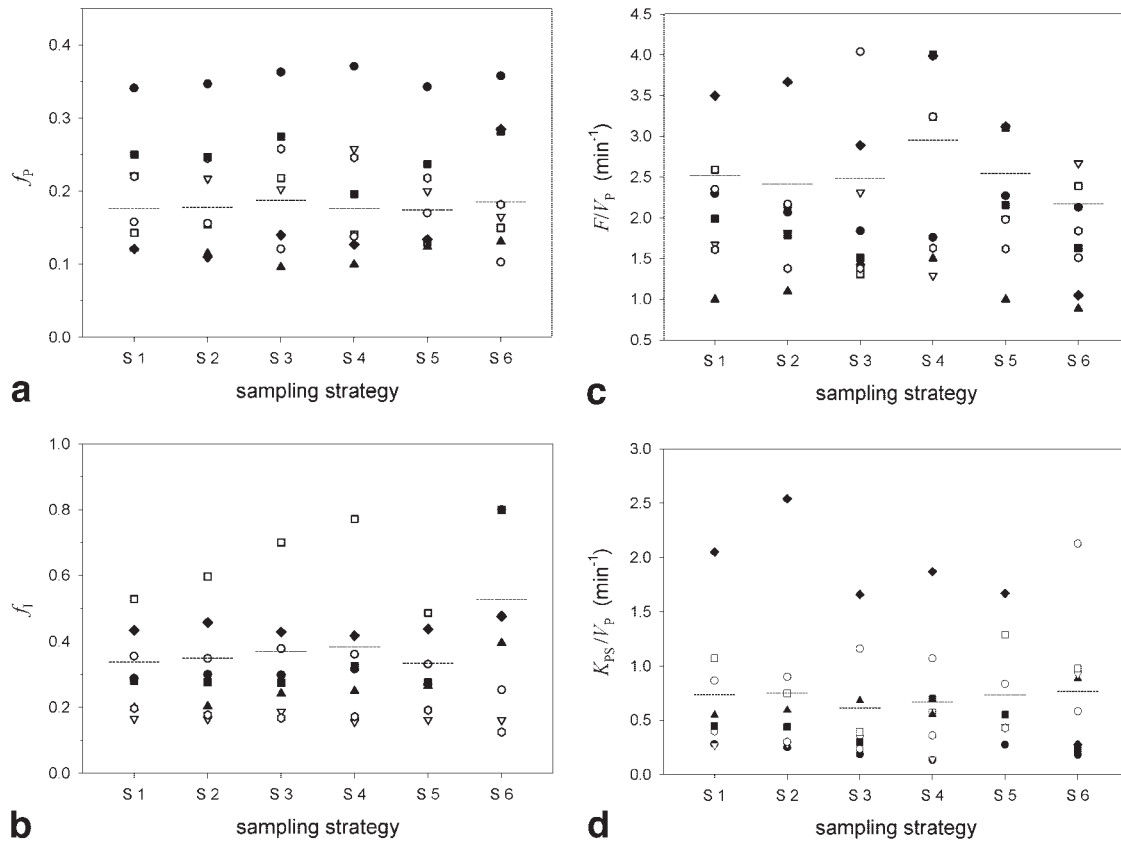


FIG. 3. Comparison of parameters estimated for eight breast carcinoma and six different sampling strategies (S1: 10.4 min/3.25 s, S2: 10.4 min/6.5 s, S3: 10.4 min/13.0 s, S4: 10.4 min/26.0 s, S5: 6.9 min/3.25 s, and S6: 3.45 min/3.25 s; for details see text). (a) f_p , (b) f_l , (c) F/V_p , and (d) K_{PS}/V_p . The symbols show the individual parameter values while the horizontal lines indicate the corresponding mean values. Please note that some data points overlap.

an individual basis with the proposed pharmacokinetic model. To overcome this limitation, individual concentration–time curves determined from blood and muscle tissue were averaged. The resulting curves are shown in Fig. 6. Pharmacokinetic analysis yielded the following tissue parameters: $f_p = 0.04 \pm 0.01$, $f_l = 0.09 \pm 0.01$, $F/V_p = 2.4 \pm 1.3 \text{ min}^{-1}$, and $K_{PS}/V_p = 1.2 \pm 0.5 \text{ min}^{-1}$. Based on these data, the following derived parameters were calculated for muscle tissue: $rBV = 5.1 \pm 1.7 \text{ ml}/100\text{g}$, $rBF = 12.5 \pm 7.8 \text{ ml}/\text{min}/100\text{g}$, $MRT_p = 25 \pm 14 \text{ s}$, and $MRT_l = 56 \pm 34 \text{ s}$.

DISCUSSION AND CONCLUSION

The method investigated in the present study offers the potential to separately characterize both capillary blood supply and tracer exchange between the plasma and the interstitial tissue compartment by means of dynamic MRI. The following discussion will focus on the two major steps of our approach: First, conversion of signal–time into concentration–time courses by an appropriate MR signal model and, second, pharmacokinetic analysis of the derived concentration–time curves.

The SRTF sequence used for breast imaging allows for the acquisition of strongly T_1 -weighted images with a high temporal and spatial resolution and thus offers the potential to detect both the fast kinetics of contrast enhancement

and lesion architecture. As demonstrated by Fig. 2, pre-contrast T_1 relaxation times can be estimated directly from the dynamic SRTF image series in order to convert measured signal–time courses into concentration–time courses according to Eq. [3]. The mean T_1 value of $1348 \pm 94 \text{ ms}$ estimated for whole blood falls into the range of mean T_1 values (1180–1470 ms) measured at 1.5 T in different studies as summarized by Barth and Moser (22). Analysis of the T_1 relaxation times of the 18 breast lesions investigated yielded somewhat lower T_1 values for carcinomas ($770 \pm 146 \text{ ms}$) than for benign lesions ($875 \pm 107 \text{ ms}$). These relaxation times, which were determined by means of the simplified approximation technique (cf. Fig. 2), are in agreement with average values of 711 ms and 857 ms reported by Hulka et al. (9) for malignant and benign breast lesions, respectively.

Besides the accuracy of tissue-specific pre-contrast T_1 relaxation times, the reliability of the signal model depends on two further assumptions: First, that differences in the relaxivity α of protons in the different tissue compartments can be neglected. Although recent studies provide evidence that relaxivities are affected by the content of macromolecules (19,23), which may differ between the various tissue compartments, the error introduced by this effect cannot be evaluated at present due to the lack of tissue-specific data. Second, that water diffusion within tissue compartments and water exchange between them is

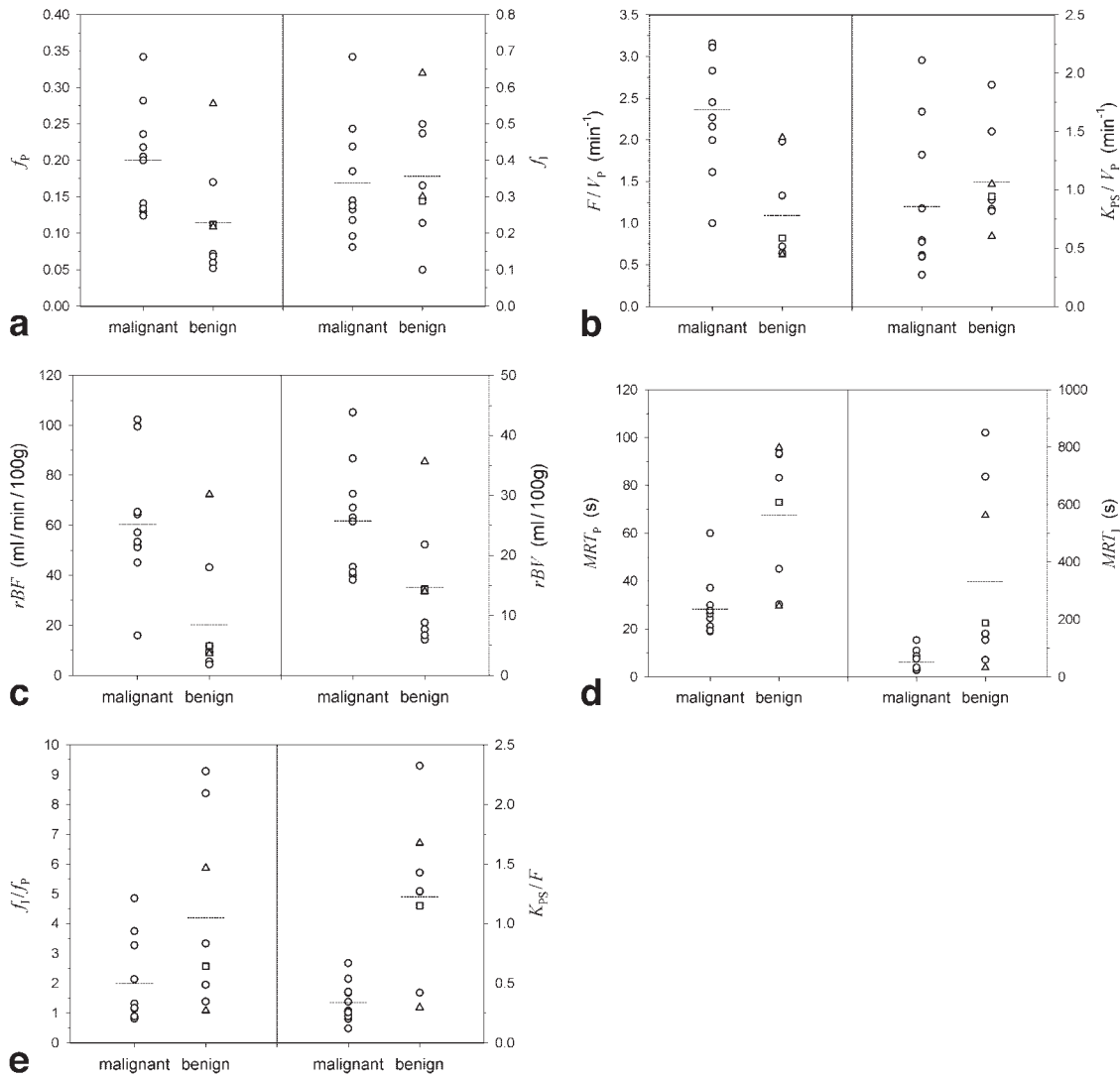


FIG. 4. Model parameters estimated for 10 malignant and 8 benign breast lesions from concentration–time curves acquired over 6.9 min with a sampling time of 3.25 s. (a) f_p and f_i , (b) F/V_p and K_{PS}/V_p , (c) rBF and rBV , (d) MRT_p and MRT_I , and (e) f_i/f_p and K_{PS}/F . The symbols show the individual parameter values while the horizontal lines indicate the corresponding mean values. The group of benign lesions comprises five histologically proven fibroadenomas (○), two fibroadenomas proven by follow-up examinations (△), and one histologically proven inflammatory lesion (□). Please note that some data points overlap.

fast enough so that the relaxation of the bulk longitudinal magnetization can be described by a single relaxation time (18).

Whether water diffusion within a compartment is fast enough so that an averaged compartmental magnetization can be assumed depends on the distance that water can diffuse during the time period between RF excitation and detection. Assuming a typical diffusion coefficient for water in soft tissues of $D = 10^{-5} \text{ cm}^2/\text{s}$, a mean net diffusion length in unbounded 3D space of $\sqrt{6 \cdot D \cdot T_{\text{REC}}} \cong 27 \mu\text{m}$ is derived for a recovery time of $T_{\text{REC}} = 125 \text{ ms}$ (18,24). This distance is comparable with the dimension of a medium-sized mammalian cell but less than the mean intercapillary distance of $49 \mu\text{m}$ measured in a mammary adenocarcinoma (25). However, to accurately determine the time it needs for a given volume element to equilibrate with its surrounding, it is necessary to solve the 3D diffusion equa-

tion under the appropriate boundary and initial conditions. For a spherical volume element of diameter $60 \mu\text{m}$, for example, it takes about 30 ms to equilibrate with a surrounding medium whose particle concentration is constant if the initial content of small particles in the sphere is zero (26). It is thus a realistic assumption that water molecules diffuse quickly enough to be sufficiently well mixed in each tissue compartment during the recovery time of 125 ms.

More critical, however, is water transport across compartmental boundaries. The relevance of boundaries depends on the rate of water exchange across the membrane relative to the difference in the relaxation rates between the compartments. Based on the exchange rates presented in a review article by Donahue et al. (18) and the concentration–time courses computed in this study, red blood cells and plasma can be described as a single vascular

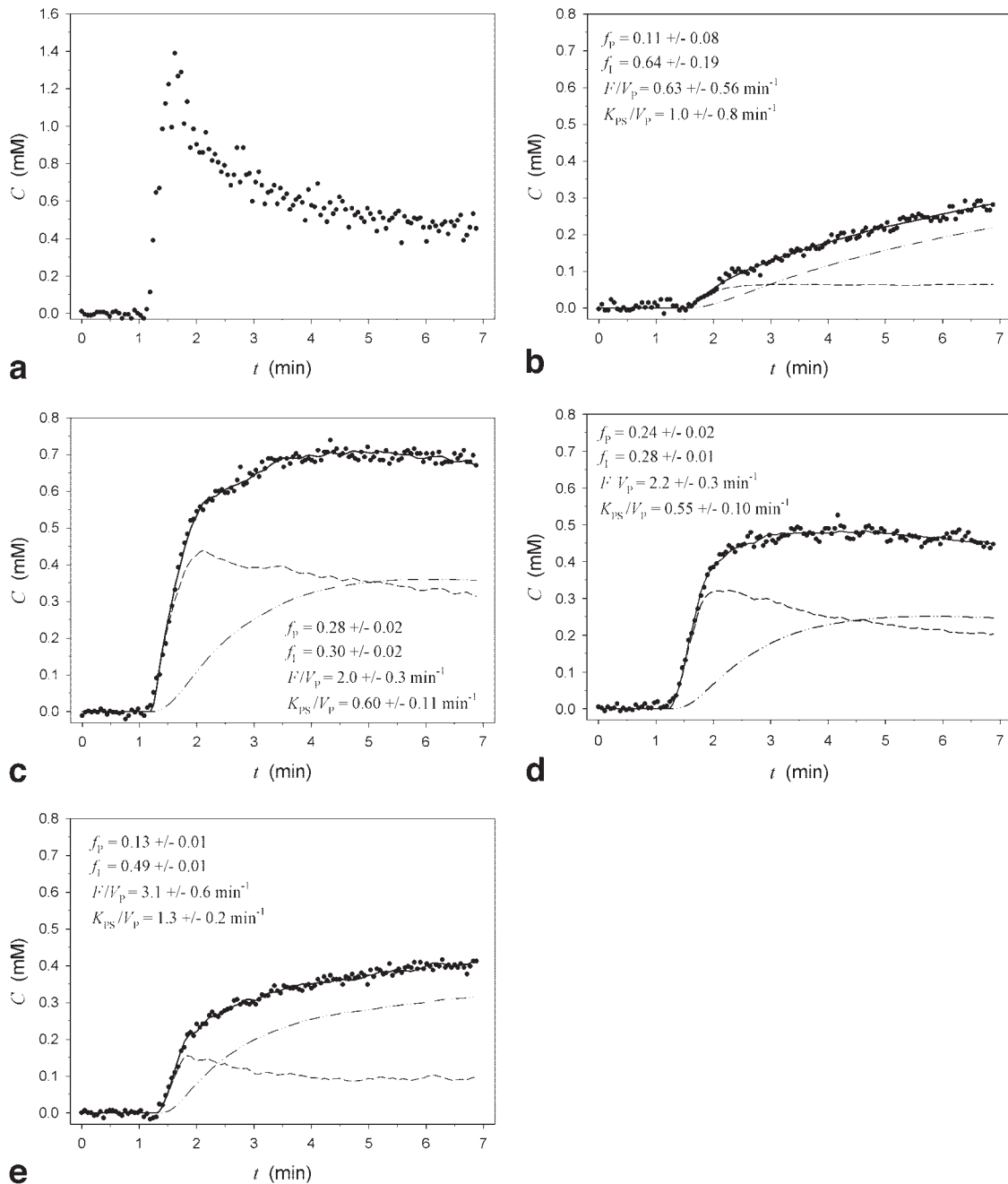


FIG. 5. Representative concentration-time curves determined from (a) the aorta, (b) a fibroadenoma with low and slow contrast enhancement, (c) a fibroadenoma with high and fast contrast enhancement, (d) a low differentiated lobular invasive carcinoma, and (e) a low differentiated ductal invasive carcinoma. The symbols show the experimentally determined concentrations, whereas the curves give the results of the pharmacokinetic analysis (solid line: total tissue concentration, C_T ; dashed line: intravascular contribution, $f_p \cdot C_p$; dash-dot line: interstitial contribution, $f_i \cdot C_i$).

compartment with a uniform relaxation rate. The same holds true for parenchymal cells and the interstitial fluid, which can be described as a uniform extravascular compartment. The difference between the relaxation rates estimated for these two compartments on the basis of the computed concentration-time curves and T_1 relaxation rates, however, reaches values of up to 5 s^{-1} in the examined breast lesions at the end of the perfusion phase, where the CM concentration in blood is highest. Since this

value is comparable with the exchange rates of $1\text{--}7 \text{ s}^{-1}$ given in the mentioned review article for normal tissues, water exchange between the vascular and extravascular compartment is in the intermediate-exchange regime at that point in time in breast tumors. Taking all aspects into account, it can be concluded that under the experimental conditions realized in our patient study, diffusion of water within and between tissue compartments is intermediate to fast. Unfortunately, there are no specific data available

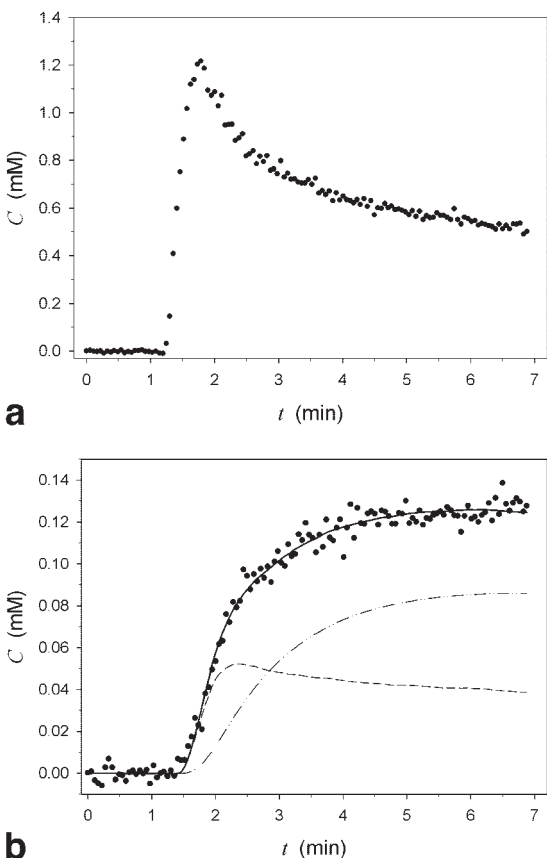


FIG. 6. Concentration–time courses determined from (a) the aorta and (b) the pectoral muscle. Data were averaged after aligning the individual curves in a way that the initial increase of the blood curves occurs at the same point in time. For details, see Fig. 5.

that characterize water exchange in breast tumors, and thus it is, at present, not possible to assign the exchange regime more precisely. Therefore, the reliability of our approach has to be assessed on the basis of the estimated tissue parameters.

The paramagnetic CM was administered in our study over a period of 30 s, which is longer than the circulation time of blood of about 20 s. For this reason, the CM is well mixed in larger arteries. This is verified by the measured blood curves presented in Figs. 5a and 6a, which show a nearly linear increase during the constant-rate CM administration over 30 s, followed by a decrease immediately after its end. Quantitatively comparable blood-curves were observed in a previous CT study after administration of the low-molecular-weight contrast agent iopromide over 30 s (16). The mean peak Gd-DTPA concentration at the end of the administration phase was 1.2 ± 0.2 mM. This value is only slightly below the blood concentration of 1.4 mM calculated for a standard person (body weight, 70 kg; blood volume, 5 l) after administration of 0.1 mmol/kg-bw Gd-DTPA under the assumption that extravasation can be neglected.

Data presented in Fig. 3 indicate that it is a reasonable compromise between accuracy of parameter estimation and practicality of the measurement procedure in clinical routine to acquire dynamic MR data over 6.9 min with a

sampling time of 3.25 s (strategy S5). Doubling the sampling time from 3.25 to 6.5 s (strategy S2) or increasing the total measurement period from 6.9 to 10.4 min (strategy S1) yielded tissue parameters which differ in average less than 10.8% and 8.4%, respectively. Further reduction of the temporal resolution or especially of the total measurement time, however, resulted in large errors in the fitted tissue parameters and is thus inadequate for quantitative analysis of functional processes in breast lesions.

A basic assumption of pharmacokinetic models is that compartments are well stirred, which means that any CM entering a compartment is instantaneously distributed throughout its entire volume. Whereas this is a good approximation for the interstitial space, it is a crude simplification of the complex situation in capillaries, because spatial variations of the CM concentration along microvessels are neglected (27,28). For this reason, axially distributed capillary models have been developed (29). These complex models, however, have too many confounding parameters generally not known for tumor tissue. On the other hand, the simplifying assumption of a well-stirred capillary compartment used in our approach may result in numerical estimates for the transport parameter K_{PS} that differ from the permeability surface area product, PS , determined by axillary distributed capillary models.

To assess the validity of our compartment approach, concentration–time courses measured from the pectoral muscle were analyzed. The mean values estimated for blood volume (5.1 ± 1.7 ml/100g) and blood flow (12.5 ± 7.8 ml/min/100g) are above the range of blood volume (1.8–4.7 ml/100g) and blood flow (2–7 ml/min/100g) data determined for resting muscle tissue by PET or plethysmography (references quoted in Ref. 16). This discrepancy may be explained—at least in part—by the fact that pectoral muscles were not examined under resting conditions in our study since the patients lay prone on the muscle with the arms extended above the head. It is interesting to note, on the other hand, that the mean values determined in the present study for pectoral muscle tissue are nearly identical with mean values of $rBV = 4.9 \pm 1.3$ ml/100g and $rBF = 12.0 \pm 5.4$ estimated for human neck muscle by dynamic CT upon administration of the nonionic CM iopromide by means of the same pharmacokinetic model and software implementation as used in the present study (16). Since contrast-enhanced CT measurements are not affected by water exchange, the good agreement between the functional parameters determined with dynamic CT and MRI for muscle tissue makes a strong argument that MR data can be analyzed under the assumption of fast-exchange conditions for this type of tissue and the measurement conditions realized. The relative fractions of the plasma ($f_p = 0.04 \pm 0.01$) and interstitial tissue compartment ($f_i = 0.09 \pm 0.01$) also coincide well with the scarce literature data available for muscle tissue. For skeletal muscle of the rat, Gullino et al. (30) and O'Connor and Bale (31) reported a relative fraction of the interstitial volume of 0.16 ± 0.07 and 0.14 ± 0.02 , respectively. Appelgren et al. (32) give a relative volume of the extracellular space ($\approx f_p + f_i$) of 0.13.

Figure 4a reveals that both plasma and interstitial space in the examined breast carcinomas are much larger than in muscle tissue (f_p : 0.20 ± 0.07 vs. 0.04 ± 0.01 ; f_i : $0.34 \pm$

0.16 vs. 0.09 ± 0.01). The estimated interstitial tumor volumes are consistent with mean values of $f_i = 0.33\text{--}0.60$ summarized in a comprehensive review article by Jain (33) for a variety of experimental sarcoma and carcinoma of the rat.

Only a few studies on blood flow through breast tumors in humans have been reported so far. Data published to 2000 are summarized in a review article by Vaupel and Höckel (6). Despite similar histological classification and primary site, the reported blood flow values vary considerably between 8 and 80 ml/min/100g. In more recent studies using PET and O-15-labeled water, whole-tumor blood flow in breast carcinomas was determined to be 14.9 ± 2.5 ml/min/100g (34) and 30 ± 14 ml/min/100g (35). Compared to these data, the blood flow of 61 ± 25 ml/min/100g measured in the present study for 10 untreated carcinomas is in the upper range. It should be noted, however, that we did not determine blood flow in the whole tumor but rather in tumor regions with the highest and fastest contrast enhancement. Moreover, limitations in the temporal and spatial resolution of dynamic PET measurements in patients can result in a systematic underestimation of blood flow.

In an experimental study, Daldrup et al. (12) measured microcirculation in R3230 mammary adenocarcinoma implanted in the mammary fat pads of rats using Gd-DTPA as tracer. This investigation yielded mean values of $f_p = 0.08 \pm 0.02$, $F/V_p = 3.0 \pm 1.1 \text{ min}^{-1}$, and $K_{PS}/V_p = 0.6 \pm 0.2 \text{ min}^{-1}$. Taking into account that the implanted tumors, which were examined at an early stage of growth, may have a different microvasculature as compared to spontaneous breast carcinomas in humans, these values are in reasonable agreement with those estimated in the present study.

Best separation between benign and malignant breast lesions was obtained in our study by the ratio K_{PS}/F . This parameter was less than 1 in all carcinomas and on average greater than 1 in benign lesions. Choosing a cut-off level of $K_{PS}/F = 1$, all 10 carcinomas and 6 of 8 benign lesions were classified correctly. However, larger prospective patient studies are required to validate the clinical relevance of the parameter K_{PS}/F for differential diagnosis of breast lesions. From a physiological point of view, the data presented in Fig. 4e reveal that contrast enhancement in hot spots of breast carcinomas is permeability-limited, whereas in 6 of 8 benign lesions it is flow-limited. It should be noted in this context that PS (and thus K_{PS}) can be higher than F because it defines the transport of tracer that could be achieved if capillary concentration was maintained at the arterial level throughout capillary length (36). Our results do not confirm the hypothesis of Kuhl et al. (4) that an increasing or decreasing CM concentration over about 5–6 min after the initial perfusion phase is a strong indicator for a benign and a malignant lesion, respectively (cf. Fig. 5b–e). According to our data, this pattern of concentration–time courses is primarily determined in breast lesions by the volume ratio f_i/f_p —a tissue parameter that does not discriminate between malignant and benign lesions, as demonstrated in Fig. 4e.

The pharmacokinetic properties of conventional CM make them an ideal probe for studying the chances of circulating low-molecular-weight compounds to distribute

into the interstitial space of defined tissues. This is particularly interesting for solid malignant tumors as, in this case, the transport of systemically administered drugs through the vascular and interstitial space to the target cells is one of the major problems of anticancer drug therapy (37). According to Eq. [8], the mean residence time of CM particles in the interstitial compartment, MRT_i , can be derived from model parameters fitted to the concentration–time curves. For the examined breast carcinomas, this analysis yielded a mean residence time of 52 ± 36 s, which is comparable with the value of 56 ± 34 s determined for muscle tissue.

In conclusion, the proposed pharmacokinetic analysis of dynamic MR data offers promising prospects to quantitatively characterize tissue microcirculation and microvasculature in tumors. Although our approach is not yet validated in all details, the agreement of the results with published data indicates that it can be employed to improve our understanding of tumor pathophysiology. Its impact on diagnosis and therapy management of breast tumors, however, has to be evaluated in larger patient studies.

ACKNOWLEDGMENT

We thank Dr. Gesine Hellwig and Jürgen Heiss for helpful discussions and support.

REFERENCES

- Harms SE, Flamig DP. Breast MRI. *Clin Imag* 2001;25:227–246.
- Morris EA. Breast cancer imaging with MRI. *Radiol Clin North Am* 2002;40:443–466.
- Schnall MD. Breast MR imaging. *Radiol Clin North Am* 2003;41:43–50.
- Kuhl CK, Mielcareck P, Klaschik S, Leutner C, Wardelmann E, Gieseke J, Schild HH. Dynamic breast MR imaging: are signal intensity time course data useful for differential diagnosis of enhancing lesions? *Radiology* 1999;211:101–110.
- Knopp MV, Weiss E, Sinn HP, Mattern J, Junkermann H, Radeleff J, Magener A, Brix G, Delorme S, Zuna I, van Kaick G. Pathophysiologic basis of contrast enhancement in breast tumors. *J Magn Reson Imag* 1999;10:260–266.
- Vaupel P, Höckel M. Blood supply, oxygenation status and metabolic micromilieu of breast cancers. Characterization and therapeutic relevance. *Int J Oncol* 2000;17:869–879.
- Hoffmann U, Brix G, Knopp MV, Heß Th, Lorenz WJ. Pharmacokinetic mapping of the breast: a new method for dynamic MR mammography. *Magn Reson Med* 1995;33:506–514.
- Tofts PS, Berkowitz B, Schnall MD. Quantitative analysis of dynamic Gd-DTPA enhancement in breast tumors using a permeability model. *Magn Reson Med* 1995;33:564–568.
- Hulka CA, Smith BL, Sgroi DC, Tan L, Edmister WB, Semple JP, Campbell T, Kopans DB, Brady TJ, Weisskoff RM. Benign and malignant breast lesions: differentiation with echo-planar MR imaging. *Radiology* 1995;197:33–38.
- Hulka CA, Edmister WB, Smith BL, Tan LT, Sgroi DC, Campbell T, Kopans DB, Weisskoff RM. Dynamic echo-planar imaging of the breast: experience in diagnosing breast carcinoma and correlation with tumor angiogenesis. *Radiology* 1997;205:837–842.
- den Boer JA, Hoenderop RKKM, Smink J, Dornseiffen G, Koch PWAA, Mulder JH, Slump CH, Volker EDP, de Vos RAI. Pharmacokinetic analysis of Gd-DTPA enhancement in dynamic three-dimensional MRI of breast lesions. *J Magn Reson Imag* 1997;7:702–715.
- Daldrup HE, Shames DM, Husseini W, Wendland MF, Okuhata Y, Brasch RC. Quantification of the extraction fraction for gadopentetate across breast cancer capillaries. *Magn Reson Med* 1998;40:537–543.
- Port RE, Knopp MV, Hoffmann U, Zabel S, Brix G. Multicompartment analysis of gadolinium chelate kinetics: blood-tissue exchange in mammary tumors as monitored by dynamic MR imaging. *J Magn Reson Imag* 1999;10:233–241.

14. Henderson E, Sykes J, Drost D, Weinmann HJ, Rutt BR, Lee TY. Simultaneous MRI measurements of blood flow, blood volume, and capillary permeability in mammary tumors using two different contrast agents. *J Magn Reson Imag* 2000;12:991–1003.
15. Delille JD, Slanetz PJ, Yeh ED, Kopans DB, Garrido L. Breast cancer: regional blood flow and blood volume measured with magnetic susceptibility-based MR imaging — initial results. *Radiology* 2002;223:558–565.
16. Brix G, Bahner M, Hoffmann U, Horvath A, Schreiber W. Regional blood flow, capillary permeability, and compartment volumes: Measurement with dynamic computed tomography — initial experience. *Radiology* 1999;210:269–276.
17. Stepanow B, Blüml S, Brix G, Schad LR, Lorenz WJ. Comparison of T1 measurements by means of TurboFLASH techniques performed on a conventional whole-body MR Imager. *SMRM, 12th Scientific Meeting, 1993, Book of Abstracts, 2:742*.
18. Donahue KM, Weisskoff RM, Burstein D. Water diffusion and exchange as they influence contrast enhancement. *J Magn Reson Imag* 1997;7:102–110.
19. Mørkenborg J, Taaghehøj JF, Væver PN, Frøker, Djurhuus JC, Stødkilde-Jørgensen H. In vivo measurement of T1 and T2 relaxivities in the kidney cortex of the pig—based on a two-compartment steady-state model. *Magn Reson Imag* 1998;16:933–942.
20. Eisenfeld J. On mean residence times in compartments. *Math Biosci* 1981;57:265–278.
21. García-Meseguer MJ, Vidal de Labra JA, García-Moreno M, García-Cánovas F, Havsteen BH, Varón R. Mean residence times in linear compartmental systems. Symbolic formulae for their direct evaluation. *Bull Math Biol* 2003;65:279–308.
22. Barth M, Moser E. Proton NMR relaxation times of human blood samples at 1.5 T and implications for functional MRI. *Cell Mol Biol* 1997;43:783–791.
23. Stanisz GJ, Henkelman RM. Gd-DTPA relaxivity depends on macromolecular content. *Magn Reson Med* 2000;44:665–667.
24. Lightfoot EN, Duca KA. The roles of mass transfer in tissue function. In: Bronzino JE, editor in chief. *The biomedical engineering handbook, vol 2*. Boca Raton, FL: CRC Press; 2000.
25. Less JR, Skalak TC, Sevick EM, Jain RK. Microvascular architecture in a mammary carcinoma: branching patterns and vessel dimensions. *Cancer Res* 1991;51:265–273.
26. Weiss TF. *Cellular biophysics, vol. 1. Transport*. Cambridge, MA: MIT Press; 1995.
27. Bassingthwaite JB. A concurrent flow model for extraction during transcapillary passage. *Circ Res* 1974;35:483–503.
28. Moran GR, Prato FS. Modeling tissue contrast agent concentration: a solution to the tissue homogeneity model using a simulated arterial input function. *Magn Reson Med* 2001;45:42–45.
29. Bassingthwaite JB, Goresky CA. Modelling in the analysis of solute and water exchange in the microvasculature. In: Renkin EM, Michel CC, Geiger SR, editors. *Handbook of physiology, vol. IV, sect. 2*. Bethesda, MD: American Physiology Society; 1984. p 549–626.
30. Gullino PM, Grantham FH, Smith SH. The interstitial water space of tumors. *Cancer Res* 1965;25:727–731.
31. O'Connor SW, Bale WF. Accessibility of circulating immunoglobulin G to the extravascular compartment of solid rat tumors. *Cancer Res* 1984;44:3719–3723.
32. Appelgren L, Peterson HI, Rosengren B. Vascular and extravascular spaces in two transplantable tumors of the rat. *Bibl Anat* 1973;12:504–510.
33. Jain RK. Transport of molecules across tumor vasculature. *Cancer Metast Rev* 1987;6:559–593.
34. Zasadny KR, Tatsumi M, Wahl RL. FDG metabolism and uptake versus blood flow in women with untreated primary breast cancers. *Eur J Nucl Med* 2003;30:274–280.
35. Mankoff DA, Dunnwald LK, Gralow JR, Ellis GK, Schubert EK, Tseng J, Lawton TJ, Linden HM, Livingston RB. Changes in blood flow and metabolism in locally advanced breast cancer treated with neoadjuvant chemotherapy. *J Nucl Med* 2003;44:1806–1814.
36. Peters AM, Myers MJ. *Physiological measurements with radionuclides in clinical practice*. Oxford: Oxford University Press; 1998. p 43.
37. Jain RK. Delivery of molecular and cellular medicine to solid tumors. *Microcirculation* 1997;4:1–23.